

Barrier distributions and signatures of transfer channels in the $^{40}\text{Ca} + ^{58,64}\text{Ni}$ fusion reactions at energies around and below the Coulomb barrier

D. Bourgin,^{1,2,*} S. Courtin,^{1,2} F. Haas,^{1,2} A. M. Stefanini,³ G. Montagnoli,⁴ A. Goasduff,⁵ D. Montanari,^{1,2,6} L. Corradi,³ E. Fioretto,³ J. Huiming,³ F. Scarlassara,⁴ N. Rowley,⁷ S. Szilner,⁸ and T. Mijatović⁸

¹*IPHC, Université de Strasbourg, F-67037 Strasbourg, France*

²*CNRS, UMR7178, F-67037 Strasbourg, France*

³*INFN, Laboratori Nazionali di Legnaro, I-35020 Legnaro (Padova), Italy*

⁴*Dipartimento di Fisica, Università di Padova, and INFN, Sezione di Padova, I-35131 Padova, Italy*

⁵*CSNSM UMR8609 IN2P3-CNRS, Université Paris-Sud 11, F-91404 Orsay, France*

⁶*Institut d'Etudes Avancées de l'Université de Strasbourg, Strasbourg, France*

⁷*Institut de Physique Nucléaire, Orsay, France*

⁸*Ruder Boskovic Institute, HR-10002 Zagreb, Croatia*

(Received 4 September 2014; published 21 October 2014)

Background: The nuclear structure of colliding nuclei is known to influence the fusion process. Couplings of the relative motion to nuclear shape deformations and vibrations lead to an enhancement of the sub-barrier fusion cross section in comparison with the predictions of one-dimensional barrier penetration models. This enhancement is explained by coupled-channels calculations including these couplings. The sub-barrier fusion cross section is also affected by nucleon transfer channels between the colliding nuclei.

Purpose: The aim of the present experiment is to investigate the influence of the projectile and target nuclear structures on the fusion cross sections in the $^{40}\text{Ca} + ^{58}\text{Ni}$ and $^{40}\text{Ca} + ^{64}\text{Ni}$ systems.

Methods: The experimental and theoretical fusion excitation functions as well as the barrier distributions were compared for these two systems. Coupled-channels calculations were performed using the CCFULL code.

Results: Good agreement was found between the measured and calculated fusion cross sections for the $^{40}\text{Ca} + ^{58}\text{Ni}$ system. The situation is different for the $^{40}\text{Ca} + ^{64}\text{Ni}$ system where the coupled-channels calculations with no nucleon transfer clearly underestimate the fusion cross sections below the Coulomb barrier. The fusion excitation function was, however, well reproduced at low and high energies by including the coupling to the neutron pair-transfer channel in the calculations.

Conclusions: The nuclear structure of the colliding nuclei influences the fusion cross sections below the Coulomb barrier for both $^{40}\text{Ca} + ^{58,64}\text{Ni}$ systems. Moreover, we highlighted the effect of the neutron pair-transfer channel on the fusion cross sections in $^{40}\text{Ca} + ^{64}\text{Ni}$.

DOI: [10.1103/PhysRevC.90.044610](https://doi.org/10.1103/PhysRevC.90.044610)

PACS number(s): 25.70.Jj, 24.10.Eq

I. INTRODUCTION AND BACKGROUND STUDIES

Heavy-ion fusion cross sections near the Coulomb barrier (CB) are influenced by couplings of the relative motion of the colliding nuclei to nuclear shape deformations and vibrations [1–5]. These couplings lead to an enhancement of the sub-barrier fusion cross section with respect to one-dimensional barrier penetration expectations and can be included into coupled-channels (CC) calculations (see Ref. [6] for a recent review article). The sub-barrier fusion cross section is also affected by nucleon transfer channels between the colliding nuclei [7–10]. The effects of the couplings can be probed by extracting the barrier distribution, $B(D)$, from precise and detailed fusion data. Experimental barrier distributions are calculated [11] from the second derivative of $E_{c.m.} \times \sigma_f$ with respect to $E_{c.m.}$, where $E_{c.m.}$ and σ_f denote the center-of-mass energy and the fusion cross section, respectively. Since the second derivative generates well-defined structures, the barrier distribution displays a sensitive pattern to the projectile and target nuclear structures. More recently, fusion

reactions were studied at deep sub-barrier energies [12,13]. Hindrance of the fusion cross section, in comparison with standard CC calculations using a Woods-Saxon potential, was observed in many medium-mass systems with negative fusion Q values. The slope of the fusion excitation function keeps increasing with decreasing energies, much faster than predicted by CC calculations. The CC descriptions and the fusion hindrance phenomenon are discussed in detail in a recent review article [14].

For systems involving Ni and Ca isotopes, accurate fusion cross section measurements from well above the CB down to very low energies, to study fusion enhancement and hindrance phenomena in $^{58,64}\text{Ni} + ^{58,64}\text{Ni}$ and $^{40,48}\text{Ca} + ^{40,48}\text{Ca}$, are reported in the literature. The experimental and theoretical results can be summarized as follows.

The fusion excitation functions for $^{58}\text{Ni} + ^{58}\text{Ni}$, $^{64}\text{Ni} + ^{64}\text{Ni}$ and $^{58}\text{Ni} + ^{64}\text{Ni}$ were measured above and below the CB, and are reported in Refs. [12,15–17]. Some of the obtained results are shown in Fig. 1. At above-barrier energies, the fusion excitation functions approach one another. At far sub-barrier energies, the fusion excitation functions differ from one another by up to two orders of magnitude. The addition of neutrons results in large increases in sub-barrier

*dominique.bourgin@iphc.cnrs.fr

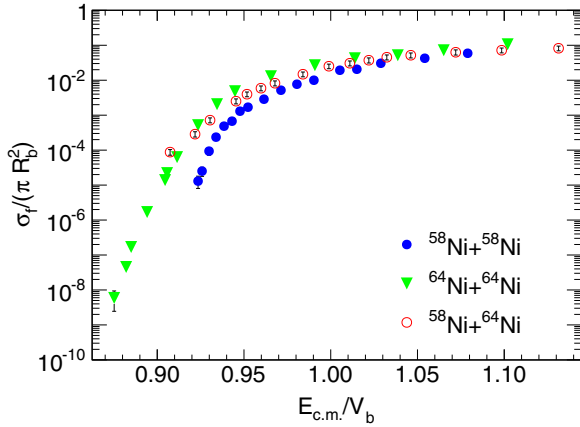


FIG. 1. (Color online) Experimental fusion excitation functions for $^{58}\text{Ni} + ^{58}\text{Ni}$ [15] (filled circles), $^{64}\text{Ni} + ^{64}\text{Ni}$ [12] (solid triangles), and $^{58}\text{Ni} + ^{64}\text{Ni}$ [17] (open circles) in reduced coordinates. R_b and V_b denote the Coulomb barrier radius and height, respectively [21].

fusion. However, the fusion excitation function for $^{58}\text{Ni} + ^{64}\text{Ni}$ descends more gradually than that for either $^{58}\text{Ni} + ^{58}\text{Ni}$ or $^{64}\text{Ni} + ^{64}\text{Ni}$. A phenomenological barrier penetration analysis was performed. Above the CB, the experimental fusion excitation functions are well reproduced. Below the CB, the calculated fusion cross sections underestimate the measured fusion cross sections.

In the case of $^{64}\text{Ni} + ^{64}\text{Ni}$ and $^{58}\text{Ni} + ^{64}\text{Ni}$, measured by Ackermann *et al.* [17], the fusion cross sections were compared with CC calculations using the CCFUS code [18]. The Akyüz-Winther (AW) nuclear potential [19] was used and couplings to the first excited 2_1^+ and 3_1^- states of the projectile and target were included. For the symmetric $^{64}\text{Ni} + ^{64}\text{Ni}$ system, where no nucleon transfer channels with positive Q value are present, the results are well reproduced by the CC calculations, whereas, in the asymmetric $^{58}\text{Ni} + ^{64}\text{Ni}$ system, the additional coupling to the neutron pair-transfer channel with a positive Q value is needed for a satisfactory agreement between measured and calculated fusion cross sections. Thus evidence for the influence of the $2n$ -transfer channel with a positive Q value on the fusion cross section was found in this asymmetric reaction case.

The fusion excitation function for $^{64}\text{Ni} + ^{64}\text{Ni}$ was measured by Jiang *et al.* [12] down to the 10 nb level, while previous measurements from Beckerman *et al.* [16] and Ackermann *et al.* [17] obtained data only down to about 20 μb . CC calculations, previously performed by Esbensen *et al.* [20] for $^{64}\text{Ni} + ^{64}\text{Ni}$ by fitting the Ackermann *et al.* data, were also performed for $^{64}\text{Ni} + ^{64}\text{Ni}$ by fitting the Jiang *et al.* data. The calculations included 2_1^+ and 3_1^- one-phonon excitations, the mutual excitation, and the two-phonon quadrupole excitation estimated within a vibrational model. The measured and calculated fusion cross sections differ at extreme sub-barrier energies and thus a fusion hindrance was proposed for this system.

Concerning the Ca + Ca systems (Fig. 2), the $^{48}\text{Ca} + ^{48}\text{Ca}$ fusion excitation function was measured by Stefanini *et al.* [22] above and well below the CB, down to $\simeq 500$ nb fusion

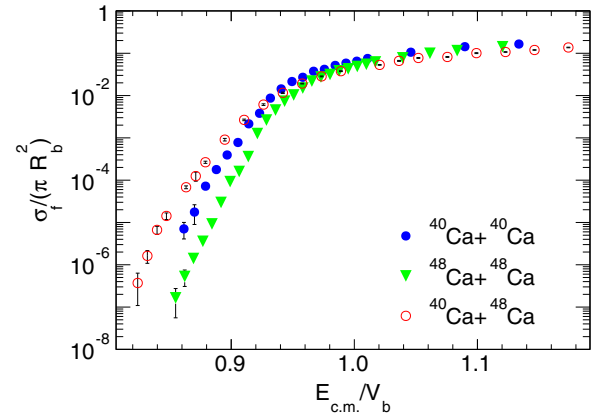


FIG. 2. (Color online) Fusion excitation functions for $^{40}\text{Ca} + ^{40}\text{Ca}$ [24] (filled circles), $^{48}\text{Ca} + ^{48}\text{Ca}$ [22] (solid triangles), and $^{40}\text{Ca} + ^{48}\text{Ca}$ [28] (open circles) in reduced coordinates. R_b and V_b denote the Coulomb barrier radius and height, respectively [21].

cross sections, thus largely extending the energy range of the previous Trotta *et al.* [23] experiment. For $^{40}\text{Ca} + ^{40}\text{Ca}$, the fusion excitation function was measured by Montagnoli *et al.* [24] from well above the CB down to low energies, where the fusion cross section reduces to $\simeq 20 \mu\text{b}$. The previous data for $^{40}\text{Ca} + ^{40}\text{Ca}$ by Aljuwair *et al.* [25] extended only down to $\simeq 200 \mu\text{b}$. Compared to $^{40}\text{Ca} + ^{40}\text{Ca}$, $^{48}\text{Ca} + ^{48}\text{Ca}$ has lower fusion cross sections below the CB since ^{48}Ca is more “stiff” than ^{40}Ca essentially because its 3_1^- state is not only at a higher excitation energy but has also a weaker octupole vibration strength. For these symmetric systems, the barrier distributions were extracted [22,24] by using the three-point difference formula [5] with an energy step of $\simeq 1.5$ MeV. The two barrier distributions have one main peak. In order to estimate the effect of 3_1^- excitations on the sub-barrier fusion cross sections, CC calculations were performed with the CCFULL code [26], using the AW nuclear potential. The calculations with one octupole-phonon excitation ($0_{\text{gs}}^+ \rightarrow 3_1^-$) in each nucleus overestimate the low-energy fusion cross sections for the two systems. CC calculations, using the M3Y+repulsion double-folding potential [27] in order to take into account the fusion hindrance effect and including couplings to low-lying excited states of the projectile and target, i.e., the 2_1^+ , 3_1^- and 5_1^- states, and to all mutual excitations of these one-phonon states, were performed. The two-quadrupole-phonon excitations were also considered, by combining energies and excitation reduced transition probabilities of the three members of the two-phonon multiplet, i.e., 0_1^+ , 2_2^+ and 4_1^+ , into one effective two-phonon excitation. These calculations are in good agreement with the $^{48}\text{Ca} + ^{48}\text{Ca}$ and $^{40}\text{Ca} + ^{40}\text{Ca}$ data and the barrier distributions are well reproduced.

Regarding the asymmetric $^{40}\text{Ca} + ^{48}\text{Ca}$ system, the fusion excitation function was extended down to 1 μb by Jiang *et al.* [28], i.e., two orders of magnitude smaller than previous data [23,25], and corresponding to an energy region where fusion hindrance is expected to appear. The fusion cross sections for $^{40}\text{Ca} + ^{48}\text{Ca}$ exceed the ones for the symmetric systems below the CB. The barrier distribution for $^{40}\text{Ca} + ^{48}\text{Ca}$ shows a tail extending towards low energies, contrary to

the ones for the symmetric systems. These two phenomena, observed on the fusion excitation function and the barrier distribution, may be an indication of the influence of couplings to nucleon transfer channels with positive Q values on the fusion cross section. CC calculations were performed, using the M3Y+repulsion potential and including identical inelastic couplings as previously mentioned. Couplings to one- and two-nucleon transfer channels with positive Q values were also included. They turned out to be essential to reproduce the large fusion cross sections below the barrier. The fusion hindrance effect is pushed down to low energies because of nucleon transfer couplings.

Based on our knowledge of Ni + Ni and Ca + Ca systems at energies around and below the CB, we decided to investigate the two ‘‘cross’’ systems $^{40}\text{Ca} + ^{58}\text{Ni}$ and $^{40}\text{Ca} + ^{64}\text{Ni}$ in this energy range. We recently performed these two reactions at INFN-Laboratori Nazionali di Legnaro (LNL) in Italy. The present measurements complement earlier studies on $^{40}\text{Ca} + ^{58}\text{Ni}$ [29], essentially at energies above the CB, and provide a detailed picture of the influence of the projectile and target nuclear structures on the fusion cross sections in both systems.

II. EXPERIMENT

The experiment was performed, using high-quality and intense $^{40}\text{Ca}^{9+,10+}$ beams (≈ 9 p nA) from the XTU Tandem accelerator, at laboratory energies ranging from $E_{\text{lab}} = 104.75$ to 153.5 MeV in steps of 1.25 MeV below the CB and 2.5 MeV above the CB. The Bass model [21] calculated Coulomb barriers in the laboratory frame for $^{40}\text{Ca} + ^{58}\text{Ni}$ and $^{40}\text{Ca} + ^{64}\text{Ni}$ at $V_b = 127.96$ and 121.33 MeV, respectively. ^{58}Ni and ^{64}Ni targets, 99.9% enriched in mass 58 and 99.6% enriched in mass 64, of $50 \mu\text{g}/\text{cm}^2$ thickness, were deposited on a $20 \mu\text{g}/\text{cm}^2$ ^{12}C backing. The evaporation residues, emitted at $\theta_{\text{lab}} = 2^\circ$, were separated from the beam by using the LNL electrostatic deflector in its upgraded setup mode [30].

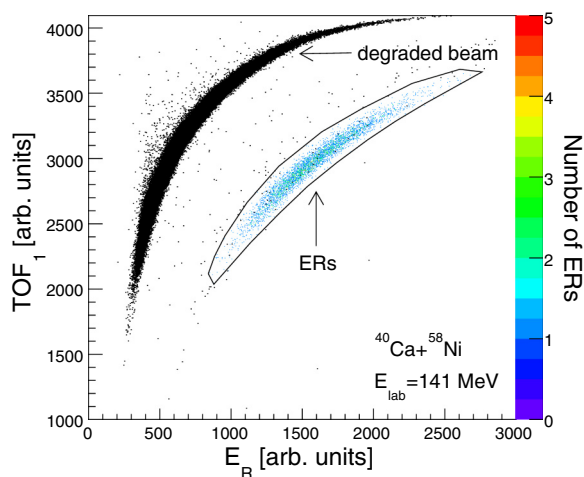


FIG. 3. (Color online) Two-dimensional spectrum of time of flight (TOF_1) vs residual energy (E_R) measured in the present experiment. The group of evaporation residues (ERs) is clearly seen and the colored points (see scale on the right) correspond to fusion events satisfying the coincidence conditions mentioned in the text.

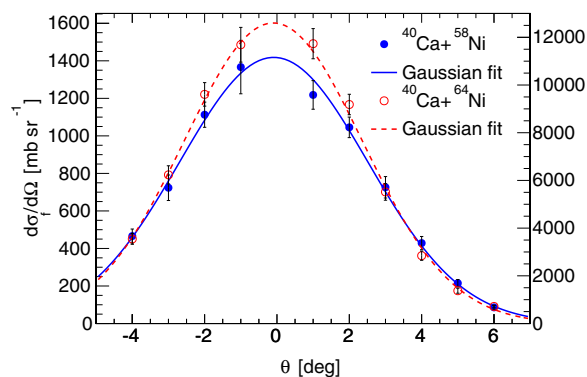


FIG. 4. (Color online) Experimental angular distributions at $E_{\text{lab}} = 121$ MeV for $^{40}\text{Ca} + ^{58}\text{Ni}$ (filled circles, scale on the left y axis) and $^{40}\text{Ca} + ^{64}\text{Ni}$ (open circles, scale on the right y axis). Gaussian fits are shown with lines.

They were first detected by two microchannel plate (MCP) detectors (position and time signals), entered then an ionization chamber (energy loss signal, ΔE) and were finally stopped in a silicon detector. The Si detector provided the residual energy E_R as well as the starting signal used for the times of flight TOF_1 (from MCP_1 to Si detector), TOF_2 (from MCP_1 to MCP_2), and TOF_3 (from MCP_2 to Si detector), and to trigger the data acquisition. The evaporation residues are identified in two-dimensional spectra, such as ΔE vs E_R , $\text{TOF}_{1,2,3}$ vs ΔE , and $\text{TOF}_{1,2,3}$ vs E_R , as shown in Fig. 3 for instance. Four silicon detectors, located above, below, and to the left and the right of the beam at the same scattering angle $\theta_{\text{lab}} \approx 16^\circ$, were used as monitors for beam control and normalization between the different runs by measuring the Rutherford scattered ^{40}Ca projectile ions. In the monitors, the elastic scattering from Ni could be easily resolved with that from the C backing due to the very different kinematical conditions of the two reactions. Two angular distributions were measured at $E_{\text{lab}} = 121$ and 138.5 MeV in the range -4° to $+6^\circ$ in steps of 1° to determine the absolute fusion cross section normalization. For instance, Fig. 4 shows the experimental angular distributions at $E_{\text{lab}} = 121$ MeV for the two systems.

III. RESULTS AND INTERPRETATION

The measured fusion cross sections for the $^{40}\text{Ca} + ^{58}\text{Ni}$ (filled circles) and $^{40}\text{Ca} + ^{64}\text{Ni}$ (open circles) systems are plotted in Fig. 5 in reduced coordinates, which allow us to compare systems with different sizes. $R_b = 10.65$ fm and $V_b = 75.73$ MeV for $^{40}\text{Ca} + ^{58}\text{Ni}$ and $R_b = 10.80$ fm and $V_b = 74.66$ MeV for $^{40}\text{Ca} + ^{64}\text{Ni}$ denote the Coulomb barrier radius and height [21]. The earlier data from Sikora *et al.* [29] for $^{40}\text{Ca} + ^{58}\text{Ni}$ (solid triangles in Figs. 5 and 6) are in good agreement with the present measurements except for the two lowest energies. It is worth mentioning that, in the Sikora *et al.* experiment, no electrostatic deflector was used. The detection system consisted in an ionization chamber and a Si detector and resulting error on these two lowest energy points was 50%. The fusion cross sections decrease regularly below the CB and the slope of the fusion excitation function for $^{40}\text{Ca} + ^{64}\text{Ni}$

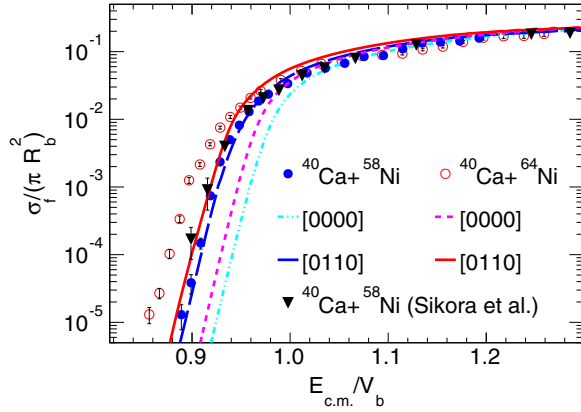


FIG. 5. (Color online) Experimental fusion excitation functions for $^{40}\text{Ca} + ^{58}\text{Ni}$ (filled circles) and $^{40}\text{Ca} + ^{64}\text{Ni}$ (open circles) in reduced coordinates. For comparison, the $^{40}\text{Ca} + ^{58}\text{Ni}$ data from Ref. [29] are also reported (solid triangles). CC calculations are shown with lines (see text for details).

is smaller (less steep) than the one of the fusion excitation function for $^{40}\text{Ca} + ^{58}\text{Ni}$ at these energies. Figure 7 shows the resulting experimental barrier distributions for the $^{40}\text{Ca} + ^{58}\text{Ni}$ (upper panel) and $^{40}\text{Ca} + ^{64}\text{Ni}$ (lower panel) systems in reduced coordinates. The reduced barrier distributions were derived from the second derivative of $(E_{c.m.} \times \sigma_f) / (\pi R_b^2)$ with respect to $E_{c.m.}$, using the three-point difference formula, with an energy step of $\Delta E_{c.m.} \simeq 1.5$ MeV below the CB and 3 MeV above the CB. These barrier distributions have a large structure centered around $E_{c.m.}/V_b \simeq 0.94$ for $^{40}\text{Ca} + ^{58}\text{Ni}$ and 0.93 for $^{40}\text{Ca} + ^{64}\text{Ni}$. According to the values of the quadrupole and octupole deformation parameters given in Table I, ^{58}Ni and ^{64}Ni have very similar nuclear structures. Despite these similarities, the barrier distribution for $^{40}\text{Ca} + ^{64}\text{Ni}$ has a longer tail towards low energies. This may result from additional reaction channels like the nucleon transfer channels. Interestingly enough, in particular, the $^{40}\text{Ca} + ^{64}\text{Ni}$ system has positive Q values for the transfer of neutrons from ^{64}Ni to

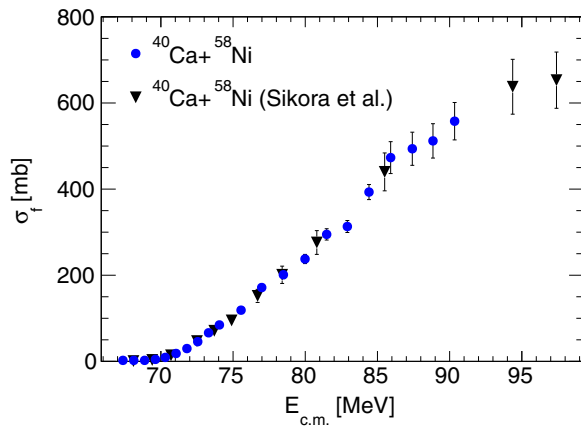


FIG. 6. (Color online) Experimental fusion excitation function for $^{40}\text{Ca} + ^{58}\text{Ni}$ (filled circles). For comparison, the $^{40}\text{Ca} + ^{58}\text{Ni}$ data from Ref. [29] are also reported (solid triangles). In this case, a linear scale is used for σ_f .

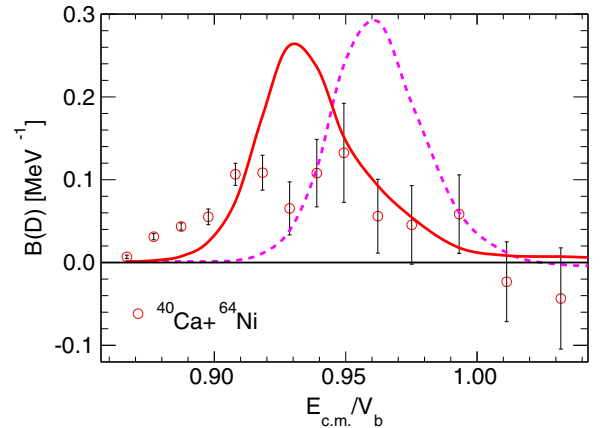
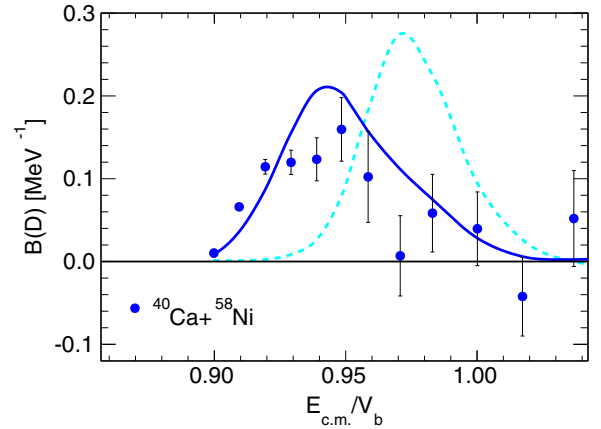


FIG. 7. (Color online) Upper panel: Experimental barrier distribution for $^{40}\text{Ca} + ^{58}\text{Ni}$ (filled circles) in reduced coordinates. Lower panel: Experimental barrier distribution for $^{40}\text{Ca} + ^{64}\text{Ni}$ (open circles) in reduced coordinates. For the two systems, CC calculations are shown with lines (see text for details).

^{40}Ca (neutron pick-up) and protons from ^{40}Ca to ^{64}Ni (proton stripping). Corresponding Q values for the two systems are listed in Table II, which shows that, for $^{40}\text{Ca} + ^{58}\text{Ni}$, all Q values are negative. The present experimental fusion excitation function and barrier distribution data are available in Ref. [31].

TABLE I. Nuclear spectroscopic informations used for ^{40}Ca , ^{58}Ni , and ^{64}Ni . The strength S of the transitions in Weisskopf units and the deformation parameters $\beta_{2,3}$ were determined from the γ -ray energies E_γ and the mean lifetimes of the states given in Ref. [32], except for the $^{58,64}\text{Ni}$ deformation parameters β_3 determined from the adopted S given in Ref. [33].

Nucleus	J^π	E_γ (keV)	S (W.u.)	$\beta_{2,3}$
^{40}Ca	3_1^-	3736	25.95	0.40
	2_1^+	3904	2.21	0.12
^{58}Ni	2_1^+	1454	9.78	0.18
	3_1^-	4475	12.6	0.20
^{64}Ni	2_1^+	1346	7.57	0.16
	3_1^-	3560	12.6	0.20

TABLE II. Corrected Q values of transfer reactions for the $^{40}\text{Ca} + ^{58,64}\text{Ni}$ systems ($Q_{\text{corr}} = Q_{\text{tr}} + V_b^{\text{in}} - V_b^{\text{out}}$) [7]. The indicated “+” sign corresponds to neutron pick-up and the “-” sign to proton stripping.

System	+1n	+2n	+3n	-1p	-2p	-3p
$^{40}\text{Ca} + ^{58}\text{Ni}$	-3.80	-2.52	-11.19	-3.75	-3.60	-11.95
$^{40}\text{Ca} + ^{64}\text{Ni}$	-1.23	3.47	0.86	0.26	4.19	0.88

We performed CC calculations with the CCFULL code, using the AW nuclear potential. The AW parameters for the $^{40}\text{Ca} + ^{58}\text{Ni}$ and $^{40}\text{Ca} + ^{64}\text{Ni}$ systems are listed in Table III. The corresponding fusion barrier positions R_b^{AW} , heights V_b^{AW} , and curvatures $\hbar\omega^{\text{AW}}$ are also listed in Table III. The CC calculations with the bare AW nuclear potential, indicated by [0000] in Fig. 5, for $^{40}\text{Ca} + ^{58}\text{Ni}$ (dotted-dashed line) and $^{40}\text{Ca} + ^{64}\text{Ni}$ (short-dashed line), give a good description of the data above the CB. Couplings are noted as $[N_{\text{quad}}^{\text{Ca}}, N_{\text{oct}}^{\text{Ca}}, N_{\text{quad}}^{\text{Ni}}, N_{\text{oct}}^{\text{Ni}}]$. N_{quad} and N_{oct} denote the number of quadrupole and octupole phonons considered in the projectile and target. With the bare potential, a deviation between the calculated and measured fusion cross sections is observed below the CB. This discrepancy can be partially explained by the influence of the nuclear structure of the colliding nuclei on the fusion process.

As can be seen in Table I, the ^{40}Ca nucleus has a large octupole deformation parameter β_3 for the first excited state 3^- and a small quadrupole deformation parameter β_2 for the first excited state 2^+ with very close excitation energies. Both ^{58}Ni and ^{64}Ni have comparable β_2 and β_3 values but the energy of the first excited state 3^- is much higher than the one of the first excited state 2^+ . Consequently, one octupole-phonon excitation for ^{40}Ca ($0_{\text{gs}}^+ \rightarrow 3_1^-$) and one quadrupole-phonon excitation for $^{58,64}\text{Ni}$ ($0_{\text{gs}}^+ \rightarrow 2_1^+$) were taken into account in CCFULL. The CC calculations with couplings are also reported in Fig. 5. The diffuseness parameter a of the AW nuclear potential was slightly increased to 0.69 fm for $^{40}\text{Ca} + ^{64}\text{Ni}$ to fit the fusion cross sections around the CB (Fig. 5) and the centroid of the barrier distribution (Fig. 7, lower panel). Increasing a leads to an enhancement of the fusion cross section in this energy range. The CC calculations for $^{40}\text{Ca} + ^{58}\text{Ni}$ (long-dashed line) are in good agreement with the data. The situation is different for $^{40}\text{Ca} + ^{64}\text{Ni}$ (solid line) where effects of nucleon transfer channels could be significant, as the calculations with no transfer clearly still underestimate

TABLE III. AW nuclear potential parameters for the $^{40}\text{Ca} + ^{58,64}\text{Ni}$ systems. V_0 , R_0 , and a denote the depth of the potential, the sum of the radii of the collision partners, and the diffuseness parameter, respectively. The corresponding fusion barrier positions R_b^{AW} , heights V_b^{AW} , and curvatures $\hbar\omega^{\text{AW}}$ are also reported.

System	V_0 (MeV)	R_0 (fm)	a (fm)	R_b^{AW} (fm)	V_b^{AW} (MeV)	$\hbar\omega^{\text{AW}}$ (MeV)
$^{40}\text{Ca} + ^{58}\text{Ni}$	67.41	8.57	0.66	10.15	73.81	3.87
$^{40}\text{Ca} + ^{64}\text{Ni}$	68.70	8.72	0.66 ^a	10.36	72.47	3.74

^a $a = 0.69$ fm was used in the CC calculations (see text for details).

the fusion cross sections below the CB. Concerning the barrier distributions shown in Fig. 7, accounting for the couplings induced a shift of $\Delta E_{\text{c.m.}}/V_b \simeq 0.03$, i.e., $\simeq 5$ MeV in the laboratory frame, towards low energies for the two systems (dashed line vs solid line). For $^{40}\text{Ca} + ^{58}\text{Ni}$, the calculated and experimental barrier distributions are also in good agreement.

The CCFULL code can schematically take into account the effect of a nucleon pair-transfer channel. This makes use of a macroscopic coupling form factor F [34] related to the ion-ion potential V_N by

$$F(r) = F_{\text{tr}} \frac{dV_N}{dr}. \quad (1)$$

Only the neutron pair-transfer channel was considered. Both parameters, Q_{tr} for the neutron pair-transfer channel Q value and F_{tr} , for the coupling strength, were treated as free parameters to obtain best agreement between the experimental and theoretical fusion excitation functions for $^{40}\text{Ca} + ^{64}\text{Ni}$. The data are well depicted at low and high energies with $Q_{\text{tr}} = 1.63$ MeV and $F_{\text{tr}} = 0.60$ fm (Fig. 8, solid line). This Q value corresponds roughly to that for an eventual neutron pair-transfer to the 1.84 MeV 0_1^+ state in ^{42}Ca . The fusion excitation function could not be well described by setting Q_{tr}

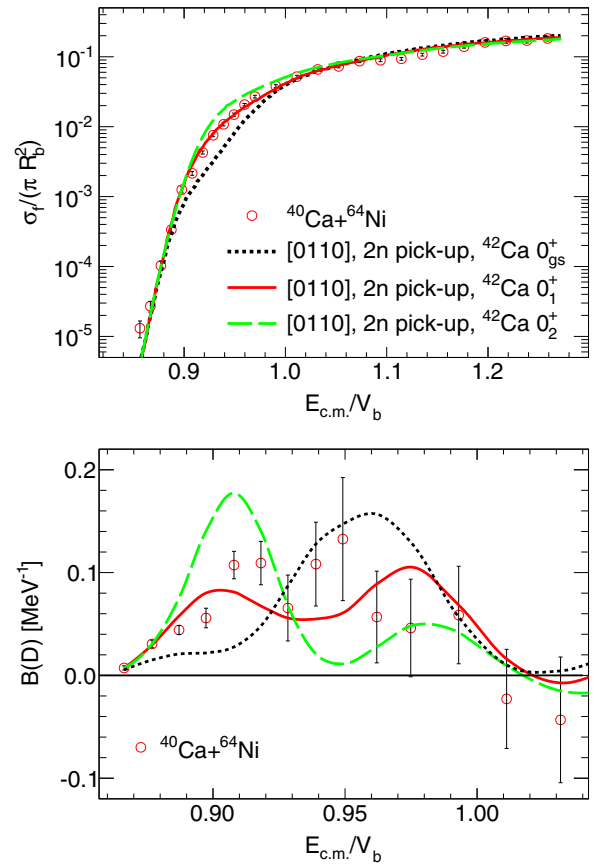


FIG. 8. (Color online) Upper panel: Reduced experimental (open circles) fusion excitation function for $^{40}\text{Ca} + ^{64}\text{Ni}$. Lower panel: Reduced experimental (open circles) barrier distribution for $^{40}\text{Ca} + ^{64}\text{Ni}$. CC calculations, including the neutron pair-transfer coupling, are shown with lines (see text for details)

to that for the neutron pair-transfer to the ground state in ^{42}Ca ($Q_{\text{tr}} = 3.47$ MeV and $F_{\text{tr}} = 0.50$ fm, dotted line) or by setting Q_{tr} to that for the neutron pair-transfer to the 3.30 MeV 0_2^+ state in ^{42}Ca ($Q_{\text{tr}} = 0.17$ MeV and $F_{\text{tr}} = 0.70$ fm, dashed line). The validity of such a calculation should be confirmed by directly measuring the nucleon pair transfers in this reaction to observe the role of other 0^+ excited states and to see if the relevant transfer cross section is consistent with the value of the coupling strength assumed above. It is worth noting that, in the case of the $^{40}\text{Ca} + ^{208}\text{Pb}$ transfer reaction to ^{42}Ca [35], the experimental results and reaction calculations pointed to a selective feeding of 0^+ states at $\simeq 6$ MeV.

IV. COMPARISON WITH Ca + Ca AND Ni + Ni SYSTEMS

As can be seen in Figs. 1 and 2, the fusion excitation functions between neutron-poor projectiles and neutron-rich targets, i.e., the asymmetric systems $^{58}\text{Ni} + ^{64}\text{Ni}$ and $^{40}\text{Ca} + ^{48}\text{Ca}$, exhibit a shallower slope than the ones for the symmetric systems. Only $^{58}\text{Ni} + ^{64}\text{Ni}$ and $^{40}\text{Ca} + ^{48}\text{Ca}$ have positive nucleon transfer Q values. The coupling to nucleon transfer channels, included into the CC calculations, for these two systems turned out to be essential for a good agreement between the measured and calculated sub-barrier fusion cross sections. The slope of the fusion excitation function was actually found to be correlated with the strength of the total neutron-transfer cross sections for systems ranging from light to heavy masses [9]. This correlation is also confirmed by the present study of the two ‘‘cross’’ systems $^{40}\text{Ca} + ^{58}\text{Ni}$ and $^{40}\text{Ca} + ^{64}\text{Ni}$. The fusion cross section for $^{40}\text{Ca} + ^{64}\text{Ni}$ (neutron-poor projectile and neutron-rich target) is larger than the ones for $^{40}\text{Ca} + ^{58}\text{Ni}$ (neutron-poor projectile and neutron-poor target) below the CB. Only $^{40}\text{Ca} + ^{64}\text{Ni}$ has positive nucleon transfer Q values. The fusion excitation function for $^{40}\text{Ca} + ^{64}\text{Ni}$ was well reproduced by including the neutron pair-transfer channel into the CC calculations. The barrier distributions for $^{40}\text{Ca} + ^{48}\text{Ca}$ and $^{40}\text{Ca} + ^{64}\text{Ni}$ both show a tail extending towards low energies. These two phenomena, brought to light by the fusion excitation function and the barrier distribution, are good indications of the influence of couplings to nucleon transfer channels with positive Q values on the fusion cross section.

V. SUMMARY

This article has reported on the measurement of the fusion excitation functions for $^{40}\text{Ca} + ^{58}\text{Ni}$ and $^{40}\text{Ca} + ^{64}\text{Ni}$ at

energies around and below the CB. Regarding $^{40}\text{Ca} + ^{58}\text{Ni}$, the CC calculations describe well the fusion cross sections above the CB without couplings and below the CB with couplings. One octupole-phonon excitation for ^{40}Ca and one quadrupole-phonon excitation for ^{58}Ni were taken into account. Regarding $^{40}\text{Ca} + ^{64}\text{Ni}$, the CC calculations described well the fusion cross sections above the CB without couplings but clearly underestimates the fusion cross sections below the CB with couplings. The same couplings were included in the CC calculations since ^{58}Ni and ^{64}Ni have very similar nuclear structures. For this system, the coupling to the neutron pair-transfer channel with a positive Q value turned out to be essential to explain the fusion cross sections below the CB with CC calculations. The barrier distributions were extracted for the two systems. The CC calculations, including the couplings, reproduced well the structure centered around $E_{\text{c.m.}}/V_b \simeq 0.94$ for $^{40}\text{Ca} + ^{58}\text{Ni}$, contrary to the structure centered around 0.93 for $^{40}\text{Ca} + ^{64}\text{Ni}$. The $^{40}\text{Ca} + ^{64}\text{Ni}$ barrier distribution, which has a longer tail towards low energies, is better reproduced by including the coupling to the neutron pair-transfer channel in the CC calculations, with a Q value corresponding to the energy of the first excited state 0_1^+ for ^{42}Ca . To summarize, nuclear structure plays a significant role in the sub-barrier fusion process for both studied systems. Nucleon transfer may also influence this process for systems with positive transfer Q values, such as $^{40}\text{Ca} + ^{64}\text{Ni}$.

A further step would be to measure fusion cross sections far below the CB for $^{40}\text{Ca} + ^{64}\text{Ni}$. This energy range would allow us to explore the influence of nucleon transfer channels on the fusion hindrance. The fusion hindrance phenomenon is predicted [36] to occur far below the Coulomb barrier for medium-mass systems with negative fusion Q values ($Q_{\text{fus}} = -17.98$ MeV for $^{40}\text{Ca} + ^{64}\text{Ni}$). Experiments to measure directly the transfer cross sections would also be of the highest interest to better understand the influence of nucleon transfer channels on $^{40}\text{Ca} + ^{58,64}\text{Ni}$.

ACKNOWLEDGMENTS

We would like to thank the professional work of the XTU Tandem and target LNL laboratory staff. The research leading to these results has received funding from the European Commission within its Seventh Framework Programme under Grant Agreement No. 262010 ENSAR. A.G. was supported by the P2IO Excellence Laboratory.

-
- [1] A. M. Stefanini *et al.*, *Phys. Rev. Lett.* **74**, 864 (1995).
 - [2] J. R. Leigh *et al.*, *Phys. Rev. C* **52**, 3151 (1995).
 - [3] J. D. Bierman, P. Chan, J. F. Liang, M. P. Kelly, A. A. Sonzogni, and R. Vandenbosch, *Phys. Rev. Lett.* **76**, 1587 (1996).
 - [4] C. H. Dasso, S. Landowne, and A. Winther, *Nucl. Phys. A* **405**, 381 (1983).
 - [5] M. Dasgupta, D. J. Hinde, N. Rowley, and A. M. Stefanini, *Annu. Rev. Nucl. Part. Sci.* **48**, 401 (1998), and references therein.
 - [6] K. Hagino and N. Takigawa, *Prog. Theor. Phys.* **128**, 1001 (2012).
 - [7] R. A. Broglia, C. H. Dasso, S. Landowne, and A. Winther, *Phys. Rev. C* **27**, 2433 (1983).
 - [8] R. A. Broglia, C. H. Dasso, S. Landowne, and G. Pollarolo, *Phys. Lett. B* **133**, 34 (1983).
 - [9] C. L. Jiang, K. E. Rehm, B. B. Back, H. Esbensen, R. V. F. Janssens, A. M. Stefanini, and G. Montagnoli, *Phys. Rev. C* **89**, 051603(R) (2014).

- [10] V. A. Rachkov, A. V. Karpov, A. S. Denikin, and V. I. Zagrebaev, *Phys. Rev. C* **90**, 014614 (2014).
- [11] N. Rowley, G. R. Satchler, and P. H. Stelson, *Phys. Lett. B* **254**, 25 (1991).
- [12] C. L. Jiang *et al.*, *Phys. Rev. Lett.* **93**, 012701 (2004).
- [13] M. Dasgupta, J. Hinde, A. Mukherjee, and J. O. Newton, *Nucl. Phys. A* **787**, 144c (2007).
- [14] B. B. Back, H. Esbensen, C. L. Jiang, and K. E. Rehm, *Rev. Mod. Phys.* **86**, 317 (2014).
- [15] M. Beckerman, J. Ball, H. Enge, M. Salomaa, A. Sperduto, S. Gazes, A. DiRienzo, and J. D. Molitoris, *Phys. Rev. C* **23**, 1581 (1981).
- [16] M. Beckerman, M. Salomaa, A. Sperduto, J. D. Molitoris, and A. DiRienzo, *Phys. Rev. C* **25**, 837 (1982).
- [17] D. Ackermann *et al.*, *Nucl. Phys. A* **609**, 91 (1996).
- [18] C. H. Dasso and S. Landowne, *Comput. Phys. Commun.* **46**, 187 (1987).
- [19] O. Akyüz and A. Winther, in *Nuclear Structure and Heavy-Ion Physics, Proceedings of the International School of Physics "Enrico Fermi", Varenna*, edited by R. A. Broglia and R. A. Ricci (North Holland, Amsterdam, 1981), p. 492.
- [20] H. Esbensen and S. Landowne, *Phys. Rev. C* **35**, 2090 (1987).
- [21] R. Bass, *Nuclear Reactions with Heavy Ions* (Springer-Verlag, Berlin, 1980).
- [22] A. M. Stefanini *et al.*, *Phys. Lett. B* **679**, 95 (2009).
- [23] M. Trotta, A. M. Stefanini, L. Corradi, A. Gadea, F. Scarlassara, S. Beghini, and G. Montagnoli, *Phys. Rev. C* **65**, 011601(R) (2001).
- [24] G. Montagnoli *et al.*, *Phys. Rev. C* **85**, 024607 (2012).
- [25] H. A. Aljuwair, R. J. Ledoux, M. Beckerman, S. B. Gazes, J. Wiggins, E. R. Cosman, R. R. Betts, S. Saini, and O. Hansen, *Phys. Rev. C* **30**, 1223 (1984).
- [26] K. Hagino, N. Rowley, and A. T. Kruppa, *Comput. Phys. Commun.* **123**, 143 (1999).
- [27] S. Misiu and H. Esbensen, *Phys. Rev. C* **75**, 034606 (2007).
- [28] C. L. Jiang *et al.*, *Phys. Rev. C* **82**, 041601(R) (2010).
- [29] B. Sikora, J. Bisplinghoff, W. Scobel, M. Beckerman, and M. Blann, *Phys. Rev. C* **20**, 2219 (1979).
- [30] A. M. Stefanini *et al.*, *Phys. Rev. C* **82**, 014614 (2010).
- [31] D. Bourgin, $^{40}\text{Ca} + ^{58}\text{Ni}$ and $^{40}\text{Ca} + ^{64}\text{Ni}$ fusion reactions, <http://sbgfusionreactions.in2p3.fr>.
- [32] National Nuclear Data Center, http://www.nndc.bnl.gov/nudat2/indx_adopted.jsp
- [33] T. Kibedi and R. H. Spear, *At. Data Nucl. Data Tables* **80**, 35 (2002).
- [34] C. H. Dasso and A. Vitturi, *Phys. Lett. B* **179**, 337 (1986).
- [35] S. Szilner *et al.*, *Eur. Phys. J. A* **21**, 87 (2004).
- [36] C. L. Jiang, H. Esbensen, B. B. Back, R. V. F. Janssens, and K. E. Rehm, *Phys. Rev. C* **69**, 014604 (2004).